

## An electron microprobe analysis, secondary ion mass spectrometry, and single-crystal X-ray diffraction study of phlogopites from Mt. Vulture, Potenza, Italy: Consideration of cation partitioning

ERNESTO MESTO,<sup>1</sup> EMANUELA SCHINGARO,<sup>1</sup> FERNANDO SCORDARI,<sup>1,\*</sup> AND LUISA OTTOLINI<sup>2</sup>

<sup>1</sup>Dipartimento Geomineralogico -Università degli Studi di Bari, Via E. Orabona 4, I-70125 Bari, Italy

<sup>2</sup>CNR-Istituto di Geoscienze e Georisorse (IGG), Sezione di Pavia, Via Ferrata, 1, I-27100 Pavia, Italy

### ABSTRACT

Mt. Vulture trioctahedral micas-1M mainly consist of phlogopite-annite solid solutions with a minor component of brittle micas. However, both Li-free and Li- and F-rich compositions may coexist in the same volcano-stratigraphic level. We report the results of electron microprobe analysis (EMPA), secondary ion mass spectrometry (SIMS), and single-crystal X-ray diffraction (SCXRD) for three crystals (LC7-27Go, LC7-3Go, and LC7-1R) that are representative of both compositions.

EMPA and SIMS showed that sample LC7-1R is richer in TiO<sub>2</sub>, Li<sub>2</sub>O, and F and poorer in H<sub>2</sub>O than the other samples.

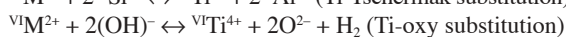
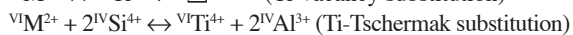
Structure refinements using anisotropic displacement parameters for the three samples, performed in space group *C2/m*, converged at  $3.46 \leq R \leq 4.34$ ,  $3.89 \leq R_w \leq 4.39$ . When considering bond distances, the three samples can be described as homo-octahedral whereas mean atomic numbers suggest that only LC7-1R is meso-octahedral. Significant differences occur among the samples for some distortion parameters commonly used for micas. In particular, LC7-1R displays higher values of BLD<sub>M2</sub>, shift<sub>M2</sub> and lower values of Δ<sub>K-04</sub> and t<sub>K-04</sub> than those of samples LC7-3Go and LC7-27Go. These differences are ascribed to F- and Ti-substitutions.

Cation distributions were obtained by combining EMPA, SIMS, and SCXRD data after analysis of the effect of normalization schemes commonly used in mica formula recalculation. In LC7-3Go and LC7-27Go, Ti is incorporated according to the Ti-Tschermak mechanism, whereas more than one Ti-substitution mechanism occurs in LC7-1R. For the latter sample, octahedral vacancies are present leading to a complex substitution pattern and complex structural distortions related to the special octahedral compositions that were determined.

**Keywords:** Analysis, chemical (mineral), EPMA and SIMS investigation, crystal structure, trioctahedral micas –1M, major and minor elements, Ti-F-bearing phlogopites, trace elements and REE, Li-bearing micas, XRD data, single-crystal structure refinement

### INTRODUCTION

Trioctahedral micas along the phlogopite-annite join are of widespread occurrence and of importance both in metamorphic and igneous environments. A detailed knowledge of their crystal chemistry is required to model the petrogenetic processes in which they participate. Unfortunately, the crystal chemistry of these mineral phases is a challenge, because of the large number of cationic, anionic substitutions and/or ordering patterns that may affect the mica structure. Much work has been devoted to the study of chemical substitutions in the octahedral sheet (see Brigatti and Guggenheim 2002, for a review), especially when high-charge cations are involved. Particular emphasis has been given to Ti in micas because of its potential as a petrogenetic indicator (Patiño Douce 1993; Henry and Guidotti 2002; Cesare et al. 2003). Incorporation of Ti in the mica structure, however, may occur in several ways, the most likely being:



This latter substitution is more common than previously suspected in magmatic and metamorphic phlogopites, as determined by recent multi-methodic studies (Virgo and Popp 2000; Righter et al. 2002; Cesare et al. 2003; Kogarko et al. 2005; Schingaro et al. 2004). In particular, a direct knowledge of the H content seems to be a fundamental step to assess the correct Ti-substitution in micas. In fact, characterization of H, Li, and F is often lacking or incomplete in micas; rarely is Secondary Ion Mass Spectrometry (SIMS) performed in silicate minerals. Despite its remarkable capabilities of detecting almost all the elements of the Periodic Table (including H) over a wide concentration range, SIMS is not a routine technique. Several artifacts affecting sputtering-ionization phenomena during a SIMS analysis need to be investigated in detail before attempting any quantitative measurement in complex geological matrixes. The interfering ions constitute a minor problem in the analysis of light elements (H, Li, B) whereas the so-called “matrix effects” seem to represent the main drawback for the other elements. An extensive investigation of SIMS analyses has been carried out in the SIMS laboratory in Pavia over the last years. The main conclusion (see Ottolini et al. 2002 and references therein) is that the matrix effects affecting SIMS ionization are mostly dependent on the chemical composition of the sample.

\* E-mail: f.scordari@geomin.uniba.it

Crystallographic orientation of the sample relative to the ion beam generally plays a minor role in producing matrix effects. This effect involves chemically reactive  $^{16}\text{O}^-$  primary ions and the ensuing amorphization of the sub-surface crystal structure. Such orientation effects are generally negligible or within the uncertainty of the SIMS analysis of light elements in silicates. However, significant influence of crystallographic orientation on  $\text{H}^+/\text{Si}^+$  was found for phengite, where a  $\sim 25\%$  difference in the ion yield for H was obtained under two extreme orientations, i.e., with the **c** and **a** axes perpendicular to the sample surface (Ottolini et al. 2002). Channeling-related processes are likely to occur when analyzing micas by ion microprobe. Recently, similar effects affecting Na/Si ionization were found in the complex layer silicate sazhnite (Ottolini et al. 2004). It is likely that an anisotropic structure is not completely destroyed during initial SIMS bombardment, eventually progressing to the formation of a continuous amorphous layer.

The Mt. Vulture trioctahedral micas-1M mainly consist of phlogopite-annite solid solutions with a minor component of brittle micas (Schingaro et al. 2001). Subsequent analysis has shown that both Li-free, Li- and F-rich compositions may coexist in the same volcano-stratigraphic level (Rinaldi 2003). In the present work, the crystal chemistry of trioctahedral micas-1M from trachytic-phonolitic deposits of Mt. Vulture was investigated by electron microprobe analysis (EMPA), Single-crystal X-ray diffraction (SCXRD), and SIMS. Our aims were (1) to perform a comparative crystal chemical analysis of Li-free and Li- and F-bearing micas-1M; (2) to determine the substitution mechanism involving Ti; and (3) to obtain the cation distribution by comparing the results of EMPA, SCXRD, and SIMS analysis.

## EXPERIMENTAL METHODS

### Sample description

The lowermost volcanic rocks of Mt. Vulture consist mainly of phonolitic-trachytic ignimbrites that are divided into two sub-units: A and B. These ignimbrites are the products of two different episodes of volcanic activity (Crisci et al. 1983; La Volpe and Principe 1989; Caggianelli et al. 1990). The micas that were studied belong to ignimbrite A deposits sampled in an outcrop at La Cupa, Potenza, Italy. A detailed stratigraphic description of the La Cupa section is reported in Balenzano et al. (1983) and in Schingaro (1993). Micas of this study all belong to the volcano-stratigraphic level no. 7 of La Cupa. At least three different populations of mica are distinguished by inspection by binocular microscope: green micas (most abundant), black micas (less abundant) and red micas (rare). Green and black micas are Ti-poor (about 2 wt%  $\text{TiO}_2$ ) and Ti-rich (about 4 wt%  $\text{TiO}_2$ ) respectively, and were studied previously by combining EMPA, Inductively Coupled Plasma (ICP), and SCXRD analyses (Schingaro et al. 2001). In the present work, three single crystals were considered: two are green micas (LC7-3Go and LC7-27Go) and one is a reddish mica (LC7-1R). The selected samples underwent chemical (EMP and SIMS) and structural (SCXRD) analyses. Particular attention was paid to the SIMS analysis of H because it may aid in determining the occurrence of  $\text{M}^{3+/4+}$ -oxy substitution in micas. Shortage of materials prevented the use of some complementary methods (i.e., Mössbauer spectroscopy for the determination of Fe speciation, and X-ray photoelectron spectroscopy for Ti speciation), which are necessary for a complete crystal-chemical characterization of such complex matrixes.

### SIMS

SIMS measurements were performed with a CAMECA IMS 4f ion microprobe installed at CNR-IGG at Pavia, Italy. A 12.5 kV  $^{16}\text{O}^-$  primary-ion beam was used with a current intensity of 1.2–2.8 nA and  $<5\ \mu\text{m}$  beam diameter. The sample mounts were washed in an ultrasonic tank with ethanol and gold coated (400 Å thickness) before the SIMS analysis. Each sample mount together with that of the standards

was left to degas overnight in the ion-microprobe sample chamber. Secondary ion signals of the following isotopes were monitored at the electron multiplier:  $^1\text{H}^+$ ,  $^7\text{Li}^+$ ,  $^9\text{Be}^+$ ,  $^{11}\text{B}^+$ ,  $^{19}\text{F}^+$ , and  $^{30}\text{Si}^+$  (the latter was used as an internal reference for the matrix). Acquisition times were 20 s (H), 10 s (Li, Be, and B), 20 s (F), and 15 s (Si) over 5 analytical cycles. Positive secondary ions with kinetic energies in the range of 75–125 eV were detected under steady-state sputtering conditions after 15 min of pre-sputtering. According to previous SIMS work on light elements in silicates, the analysis of “filtered” secondary ions is useful in reducing most chemical matrix effects and in improving the overall measurement reproducibility (Ottolini et al. 1993, 1995 and references therein). Several medium-silica silicate standards were employed for the quantification of the ion signals for H, Li, B, and F: Finero phlogopite ( $\text{SiO}_2 = 40.04\ \text{wt}\%$ , 4.20 wt%  $\text{H}_2\text{O}$ , 712 ppm F), korerupine n.6, schorl n.16, dravite n.18, and elbaite n.19 (Ottolini et al. 2002). We adopted empirical corrections to the ion yields of Li, H, and F to determine the variation of the ion signals with increasing (Fe + Mn) content in the sample. The sample mounts were then re-polished smoothly, carbon-coated, and investigated with the electron microprobe in close proximity to the SIMS craters. These EMPA data were then used in the final SIMS quantification procedures.

### EMPA

Chemical compositions were obtained from polished mineral sections with a Cameca SX-50 electron microprobe. Operating conditions were 15 kV accelerating voltage, 15 nA specimen beam current, and 10  $\mu\text{m}$  beam diameter. The analyses were performed with Wavelength Dispersive Spectrometers (WDS) for F, Na, K, Ba, Cl, and Ti, and with an energy dispersive system (EDS) LINK spectrometer for Si, Ca, Al, Mg, and Fe. The following standards were employed: jadeite (Na), periclase (Mg), wollastonite (Si and Ca), rutile (Ti), corundum (Al), magnetite (Fe), orthoclase (K), barite (Ba), fluor-phlogopite (F), sylvite (Cl). Data acquisition followed the procedure suggested by Foley (1989). A conversion from X-ray counts to oxide weight percentages was obtained with the ZAF 4/FLS data reduction system.

The results of EMPA and SIMS are listed in Table 1. SIMS spots are labeled “a” and “c” for LC7-1R, from “a” to “d” for LC7-3Go and LC7-27Go. EMPA data represent the average over about 5 spots, each spot being measured proxy to the SIMS crater. The final crystal-chemical formulae are given in Table 2.

### SCXRD

Various information about data collection and structure refinement are reported in Table 3. For samples LC7G-27Go and LC7-3Go, X-ray intensity data were collected with a HUBER single-crystal, automated four-circle diffractometer equipped with graphite-monochromated  $\text{MoK}\alpha$  (0.7107 Å) radiation at room temperature. About 1600 unique reflections [ $-450$  with  $I > 3\sigma(I)$ ] were measured with  $\pm h, \pm k, l$ , using  $\omega$  scan mode in the range  $2^\circ \leq \theta \leq 40^\circ$ . Cell parameters were refined by accurately centering 25 reflections in the range  $15^\circ \leq \theta \leq 30^\circ$ . After correction for absorption ( $\psi$ -scan, North et al. 1968) and for Lorentz and polarization effects, intensities were reduced to structure factors.

LC7-1R data collection, performed with the Huber diffractometer, resulted in an unacceptably low reflections-to-parameters ratio. We present here the results of data collection performed with the Oxford Diffraction Sapphire 2 diffractometer fitted with a Kodak KAF 1001-E CCD detector ( $\text{MoK}\alpha$  radiation) installed at the Oxford Instruments Laboratories in High Wycombe, U.K. The maximum active area diameter was 90 mm and data were collected with  $1024 \times 1024$  pixel resolution. The crystal-to-detector distance was 50 mm and 375 frames were collected with three  $\omega$  rotation runs,  $1^\circ$  scan width and an exposure of 70 s per frame. A total of 1386 reflections were measured with  $-5 \leq h \leq 6$ ,  $-10 \leq k \leq 11$ ,  $-12 \leq l \leq 12$  to  $2\theta = 55^\circ$ . These were 529 unique reflections out of which 330 yielded  $I > 3\sigma(I)$ . No absorption correction was applied because the sample was very small (see Table 3).

Anisotropic structure refinements were performed in space group  $C2/m$  using the program CRYSTALS (Watkin 1992). Starting coordinates and atom labeling were from Hazen and Burnham (1973). Ionized X-ray scattering curves were employed for non-tetrahedral cations, whereas ionized vs. neutral species were used for Si and O (Hawthorne et al. 1995). The refined parameters were scale factors, atomic positions, cation occupancy factors, and atomic displacement factors. The final  $R$ -values were in the range 3.46–4.24%.

Final atomic coordinates and displacement parameters are given in Table 4. Selected interatomic bond distances are listed in Table 5. Selected parameters commonly used to describe polyhedral and layer geometry are reported in Table 6; mean atomic numbers (m.a.n.s) as obtained from the structure refinement are compared to those calculated from chemical analyses in Table 7.

**TABLE 1.** EMPA and SIMS data (wt%) for the crystals studied

Sample name	LC7-1R 1M a	LC7-1R 1M c	LC7-3Go 1M a	LC7-3Go 1M b	LC7-3Go 1M c	LC7-3Go 1M d	LC7-27Go 1M a	LC7-27Go 1M b	LC7-27Go 1M c	LC7-27Go 1M d
SiO <sub>2</sub>	32.85	34.35	35.30	35.74	36.12	35.85	36.31	38.02	38.03	36.34
Al <sub>2</sub> O <sub>3</sub>	14.99	15.65	16.29	16.55	16.60	16.52	16.61	15.20	15.30	17.27
MgO	13.82	14.78	19.03	19.59	19.72	19.47	21.67	22.54	22.64	21.37
FeO	13.93	14.08	8.34	8.46	8.38	8.35	5.66	5.23	5.53	6.08
TiO <sub>2</sub>	5.34	5.39	2.66	2.67	2.85	2.75	1.20	0.88	0.95	1.26
K <sub>2</sub> O	7.88	8.22	8.84	8.94	8.93	8.86	9.53	9.75	9.63	9.57
Na <sub>2</sub> O	0.89	0.82	0.72	0.75	0.76	0.73	0.32	0.33	0.33	0.33
BaO	1.56	1.63	0.67	0.74	0.69	0.65	1.25	0.92	0.91	1.29
Li <sub>2</sub> O†	0.10	0.14	–	–	–	–	–	0.01	0.01	0.01
F	1.18	0.88	0.33	0.64	–	–	1.18	1.27	1.39	1.08
F†	2.13	3.51	0.49	0.51	0.52	0.52	1.62	1.98	1.94	1.60
Cl	0.12	0.12	0.01	–	–	0.04	0.01	–	–	–
H <sub>2</sub> O†	3.17	2.17	3.77	3.61	3.47	3.47	3.57	3.53	3.43	3.27
Total	96.78	100.86	96.12	97.56	98.04	97.25	97.75	98.39	98.70	98.39
O = F	0.90	1.48	0.21	0.21	0.22	0.22	0.68	0.83	0.82	0.67
O = Cl	0.03	0.03	–	–	–	–	–	–	–	–
Total	95.85	99.35	95.91	97.35	97.82	97.02	97.07	97.56	97.88	97.72
Si	2.58	2.61	2.67	2.67	2.69	2.69	2.69	2.78	2.78	2.69
Al	1.39	1.39	1.33	1.33	1.31	1.31	1.31	1.22	1.22	1.31
ΣT	3.97	4	4	4	4	4	4	4	4	4
Mg	1.62	1.67	2.15	2.18	2.19	2.18	2.39	2.46	2.47	2.35
Al	–	0.01	0.12	0.13	0.14	0.15	0.14	0.09	0.10	0.19
Fe <sup>2+</sup>	0.91	0.90	0.53	0.53	0.52	0.52	0.35	0.32	0.34	0.38
Ti	0.32	0.31	0.15	0.15	0.16	0.16	0.07	0.05	0.05	0.07
Li	0.02	0.02	–	–	–	–	–	–	–	–
ΣO	2.87	2.91	2.95	2.99	3.01	3.01	2.95	2.92	2.96	2.99
K	0.79	0.80	0.85	0.85	0.85	0.85	0.90	0.91	0.90	0.90
Na	0.14	0.12	0.11	0.11	0.11	0.11	0.05	0.05	0.05	0.05
Ba	0.05	0.05	0.02	0.02	0.02	0.02	0.04	0.03	0.03	0.04
ΣI	0.98	0.97	0.98	0.98	0.980	0.98	0.99	0.99	0.98	0.99
F	0.53	0.84	0.12	0.12	0.12	0.12	0.38	0.46	0.45	0.37
Cl	0.02	0.02	–	–	–	0.01	–	–	–	–
OH	1.66	1.10	1.90	1.80	1.72	1.74	1.76	1.72	1.67	1.61
ΣA	2.21	1.96	2.02	1.92	1.84	1.85	2.14	2.18	2.12	1.98

Notes: – = not detected. Formulae calculated with H<sub>2</sub>O, Li<sub>2</sub>O, F SIMS data ; T = Tetrahedral ; O = Octahedral ; I = Interlayer ; A = Anion.

\* Mean values of EMPA data.

† SIMS data.

**TABLE 2.** Structural formulae of the studied trioctahedral micas

Based on 12(O OH, F, Cl)	
LC7-1R (spot c)	(K <sub>0.78</sub> Na <sub>0.12</sub> Ba <sub>0.05</sub> □ <sub>0.05</sub> )(Mg <sub>1.65</sub> Fe <sub>0.48</sub> Fe <sub>0.40</sub> Li <sub>0.02</sub> Ti <sub>0.20</sub> □ <sub>0.20</sub> Ti <sub>0.05</sub> )(Si <sub>2.56</sub> Al <sub>1.38</sub> Ti <sub>0.06</sub> )O <sub>10.04</sub> (OH <sub>1.10</sub> F <sub>0.83</sub> Cl <sub>0.02</sub> )
LC7-3Go	(K <sub>0.85</sub> Na <sub>0.11</sub> Ba <sub>0.02</sub> □ <sub>0.02</sub> )(Al <sub>0.13</sub> Mg <sub>2.18</sub> Fe <sub>0.53</sub> Ti <sub>0.16</sub> )(Si <sub>2.66</sub> Al <sub>1.34</sub> )O <sub>10.08</sub> (OH <sub>1.80</sub> F <sub>0.12</sub> )
LC7-27Go (spot d)	(K <sub>0.90</sub> Na <sub>0.05</sub> Ba <sub>0.0</sub> □ <sub>0.01</sub> )(Al <sub>0.24</sub> Mg <sub>2.35</sub> Fe <sub>0.32</sub> Ti <sub>0.07</sub> □ <sub>0.02</sub> )(Si <sub>2.68</sub> Al <sub>1.26</sub> Fe <sub>0.06</sub> )O <sub>10.02</sub> (OH <sub>1.61</sub> F <sub>0.37</sub> )
Based on 7 cations	
LC7-1R (spot c)	(K <sub>0.81</sub> Na <sub>0.12</sub> Ba <sub>0.0</sub> □ <sub>0.02</sub> )(Al <sub>0.06</sub> Mg <sub>1.69</sub> Fe <sub>0.91</sub> Li <sub>0.04</sub> Ti <sub>0.30</sub> )(Si <sub>2.64</sub> Al <sub>1.36</sub> )O <sub>10.04</sub> (OH <sub>1.10</sub> F <sub>0.84</sub> Cl <sub>0.02</sub> )
LC7-3Go	(K <sub>0.86</sub> Na <sub>0.11</sub> Ba <sub>0.02</sub> □ <sub>0.01</sub> )(Al <sub>0.13</sub> Mg <sub>2.18</sub> Fe <sub>0.53</sub> Ti <sub>0.16</sub> )(Si <sub>2.67</sub> Al <sub>1.33</sub> )O <sub>10.08</sub> (OH <sub>1.80</sub> F <sub>0.12</sub> )
LC7-27Go (spot d)	(K <sub>0.90</sub> Na <sub>0.05</sub> Ba <sub>0.0</sub> □ <sub>0.01</sub> )(Al <sub>0.25</sub> Mg <sub>2.35</sub> Fe <sub>0.34</sub> Ti <sub>0.06</sub> )(Si <sub>2.75</sub> Al <sub>1.19</sub> Fe <sub>0.06</sub> )O <sub>10.02</sub> (OH <sub>1.61</sub> F <sub>0.37</sub> )
Based on Dymek(1983)	
LC7-1R (spot c)	(K <sub>0.77</sub> Na <sub>0.12</sub> Ba <sub>0.05</sub> □ <sub>0.06</sub> )(Mg <sub>1.62</sub> Fe <sub>0.29</sub> Fe <sub>0.57</sub> Li <sub>0.02</sub> Ti <sub>0.29</sub> □ <sub>0.29</sub> )(Si <sub>2.53</sub> Al <sub>1.36</sub> □ <sub>0.11</sub> )O <sub>10.04</sub> (OH <sub>1.10</sub> F <sub>0.84</sub> Cl <sub>0.02</sub> )
LC7-3Go	(K <sub>0.84</sub> Na <sub>0.11</sub> Ba <sub>0.02</sub> □ <sub>0.03</sub> )(Al <sub>0.04</sub> Mg <sub>2.14</sub> Fe <sub>0.15</sub> Fe <sub>0.37</sub> Ti <sub>0.15</sub> □ <sub>0.15</sub> )(Si <sub>2.61</sub> Al <sub>1.39</sub> )O <sub>10.08</sub> (OH <sub>1.80</sub> F <sub>0.12</sub> )
LC7-27Go (spot d)	(K <sub>0.90</sub> Na <sub>0.05</sub> Ba <sub>0.0</sub> □ <sub>0.02</sub> )(Al <sub>0.15</sub> Mg <sub>2.33</sub> Fe <sub>0.21</sub> Fe <sub>0.17</sub> Ti <sub>0.07</sub> □ <sub>0.07</sub> )(Si <sub>2.66</sub> Al <sub>1.34</sub> )O <sub>10.02</sub> (OH <sub>1.61</sub> F <sub>0.37</sub> )

## RESULTS AND DISCUSSION

### SIMS

SIMS data (Table 1) show that sample LC7-1R is a Li-bearing phase. The sample contains more F and less H<sub>2</sub>O than the other samples. Contents of Be and B are <1 ppm. B was found to be ≤12 ppm in LC7-1R.

Inhomogeneity in the chemical composition is pronounced for sample LC7-1R (see Table 1): we obtained 3.17 H<sub>2</sub>O, 0.10 Li<sub>2</sub>O, 2.13 F wt% at spot “a”, whereas 2.17 H<sub>2</sub>O, 0.14 Li<sub>2</sub>O, and 3.51 F wt% at spot “c”. The small size of the stick-shaped grains prevented an extensive SIMS investigation; moreover, some sample

areas were not suitable for ion microprobe analysis owing to the presence of micro-cracks and surface roughness. When combining EMPA with SIMS analysis, the micro-volumes involved in the production of X-rays and secondary ions never match exactly. The X-rays emitted during an e-beam bombardment come from a few micrometers depth, whereas the secondary analytical ions are produced by a shallower depth (<1 μm). Finally, repolishing the sample surface to eliminate the gold coating before final electron microprobe analysis may contribute to variations in sample composition. For these reasons, the suggestion of an uncertainty for H and F concentrations near 10–15% relative is a realistic estimation. Similar considerations hold for Li.

**TABLE 3.** Refined cell parameters and data-collection parameters for crystals studied by single-crystal XRD

Sample name	LC7-1R 1M	LC7-3Go 1M	LC7-27Go 1M
Crystal dimensions (mm)	0.06 × 0.06 × 0.001	0.23 × 0.37 × 0.008	0.17 × 0.23 × 0.015
Crystal system	Monoclinic	Monoclinic	Monoclinic
Space group	C2/m	C2/m	C2/m
Unit-cell dimension			
<i>a</i> (Å)	5.310(1)	5.315(1)	5.346(1)
<i>b</i> (Å)	9.193(2)	9.209(1)	9.257(3)
<i>c</i> (Å)	10.096(4)	10.226(3)	10.312(3)
$\alpha$ (°)	90	90	90
$\beta$ (°)	100.00(3)	99.97(3)	99.97(2)
$\gamma$ (°)	90	90	90
Volume (Å <sup>3</sup> )	485.36(24)	492.96(19)	502.61(21)
$\theta$ range for data collection (°)	4 to 27	2 to 40	2 to 40
Reflections collected/unique/ <i>R</i> merging [ <i>R</i> <sub>int</sub> ] (%)	1386/529/9.48	3233/1614/4.63	3329/1658/2.29
Final <i>R</i> [ <i>I</i> > 3 $\sigma$ ( <i>I</i> )] <i>R</i> <sub>1</sub> / <i>wR</i> (%)	4.24/4.39	3.46/3.89	3.90/4.22
$\Delta\rho_{\min}/\Delta\rho_{\max}$ (e/Å <sup>3</sup> )	-0.56/0.66	-0.89/1.19	-0.65/0.58

**TABLE 4.** Crystallographic coordinates and displacement parameters of the studied micas

Atom	<i>x/a</i>	<i>y/b</i>	<i>z/c</i>	<i>U</i> <sub>iso</sub>	<i>U</i> <sub>11</sub>	<i>U</i> <sub>22</sub>	<i>U</i> <sub>33</sub>	<i>U</i> <sub>12</sub>	<i>U</i> <sub>13</sub>	<i>U</i> <sub>23</sub>
Sample LC7-1R										
K	0	0	0	0.028(4)	0.027(2)	0.024(2)	0.032(3)	0	0.004(2)	0
T	0.5735(3)	0.1674(2)	0.2230(2)	0.013(2)	0.012(1)	0.011(1)	0.015(1)	-0.000(1)	0.0027(8)	-0.001(1)
M1	0	0.5	0.5	0.010(4)	0.011(2)	0.006(2)	0.019(3)	0	0.005(2)	0
M2	0	0.8431(3)	0.5	0.010(2)	0.008(1)	0.012(1)	0.012(1)	0	-0.0001(9)	0
O1	0.824(1)	0.2292(6)	0.1643(5)	0.024(5)	0.024(3)	0.023(3)	0.025(3)	-0.003(2)	0.004(2)	-0.003(3)
O2	0.515(1)	0	0.1666(8)	0.022(8)	0.025(4)	0.018(4)	0.023(5)	0	-0.001(3)	0
O3	0.6285(9)	0.1688(6)	0.3901(5)	0.014(4)	0.012(2)	0.011(2)	0.019(3)	-0.001(2)	0.002(2)	-0.001(3)
O4	0.135(1)	0	0.4007(7)	0.010(7)	0.014(4)	0.016(4)	0.005(4)	0	0.001(3)	0
Sample LC7-3Go										
K	0	0	0	0.032(3)	0.038(2)	0.035(2)	0.024(2)	0	0.004(1)	0
T	0.5754(3)	0.1669(2)	0.2267(1)	0.0088(12)	0.0080(6)	0.0092(7)	0.0092(7)	0.000(1)	0.0011(5)	-0.000(1)
M1	0	0.5	0.5	0.012(3)	0.013(2)	0.011(2)	0.014(2)	0	0.003(1)	0
M2	0	0.8338(3)	0.5	0.011(2)	0.009(1)	0.010(1)	0.013(1)	0	0.0021(9)	0
O1	0.8318(8)	0.2238(5)	0.1699(4)	0.016(3)	0.016(2)	0.022(2)	0.012(2)	-0.002(2)	0.003(1)	-0.003(2)
O2	0.505(1)	0	0.1701(6)	0.016(5)	0.028(3)	0.012(3)	0.013(3)	0	-0.004(2)	0
O3	0.6311(7)	0.1668(5)	0.3923(4)	0.010(3)	0.008(2)	0.010(2)	0.014(2)	0.000(2)	0.001(1)	-0.001(2)
O4	0.131(1)	0	0.3974(6)	0.010(6)	0.015(4)	0.009(3)	0.007(3)	0	0.002(3)	0
Sample LC7-27Go										
K	0	0	0	0.031(3)	0.034(2)	0.032(2)	0.027(2)	0	0.004(1)	0
T	0.5758(2)	0.1666(2)	0.2274(1)	0.0131(12)	0.0123(6)	0.0130(7)	0.0145(7)	-0.0012(8)	0.0026(5)	0.0003(9)
M1	0	0.5	0.5	0.011(3)	0.010(2)	0.010(2)	0.015(2)	0	0.004(1)	0
M2	0	0.8324(3)	0.5	0.012(2)	0.010(1)	0.012(1)	0.014(1)	0	0.0004(8)	0
O1	0.8316(7)	0.2250(5)	0.1701(4)	0.023(3)	0.024(2)	0.027(2)	0.020(2)	-0.004(2)	0.006(1)	-0.002(2)
O2	0.507(1)	0	0.1702(5)	0.021(5)	0.029(3)	0.022(3)	0.014(3)	0	-0.001(2)	0
O3	0.6302(6)	0.1667(5)	0.3924(4)	0.016(3)	0.015(2)	0.014(2)	0.018(2)	0.001(2)	0.001(1)	0.001(2)
O4	0.133(1)	0	0.3989(6)	0.016(5)	0.017(3)	0.016(3)	0.017(3)	0	0.004(2)	0

**EMPA**

Electron microprobe chemical analyses (Table 1) indicate sharp chemical differences between the green and red micas and variability within the green micas. In particular, red micas have a lower content of Mg (about 1.6 apfu.) and  $X_{\text{Mg}} = 0.65$  as compared to green micas (about 2.30 apfu and  $X_{\text{Mg}}$  about 0.85) and also a higher amount of Fe and Ti. The F content is variable among and within the three samples. Table 1 shows that F from EMPA is generally underestimated. A similar discrepancy in the experimental data for F was found in humite-group minerals (Ottolini et al. 2000). Concentrations of Cl in the samples studied are close to the detection limits (190 ppm) by EMPA, with the exception of LC7-1R. Accordingly, Cl was considered in the derivation of the formulae only for LC7-1R.

**Crystal chemistry**

Formulae recalculation is not a trivial task in the micas because several normalization schemes may be used. Each scheme may introduce artifacts in the formulae, such as underestimation or overestimation of octahedral and tetrahedral cations (see

**TABLE 5.** Selected bond distances (Å)

	LC7-1R	LC7-3Go	LC7-27Go
T-O1	1.648(5)	1.656(4)	1.671(4)
T-O1'	1.654(6)	1.663(4)	1.671(4)
T-O2	1.652(4)	1.662(3)	1.669(3)
T-O3	1.661(5)	1.668(4)	1.676(4)
<T-O>	1.654	1.662	1.672
M1-O4(×2)	2.022(7)	2.058(7)	2.056(6)
M1-O3(×4)	2.090(5)	2.079(5)	2.089(4)
<M1-O>	2.067	2.072	2.078
M2-O4(×2)	1.962(5)	2.045(5)	2.063(4)
M2-O3(×2)	2.091(5)	2.076(4)	2.082(4)
M2-O3'(×2)	2.128(6)	2.081(5)	2.093(3)
<M2-O>	2.060	2.067	2.079
<M-O>	2.062	2.068	2.079
K-O1(×4)	2.933(5)	2.933(4)	2.962(4)
K-O1'(×4)	3.304(6)	3.397(4)	3.409(4)
K-O2(×2)	2.951(8)	2.935(6)	2.963(6)
K-O2'(×2)	3.313(8)	3.396(7)	3.411(6)
<K-O> <sub>inner</sub>	2.939	2.934	2.962
<K-O> <sub>outer</sub>	3.306	3.397	3.409
<K-O>	3.123	3.166	3.186

**TABLE 6.** Selected distortion parameters of the studied crystals

	LC7-1R	LC7-3Go	LC7-27Go
$t_{\text{tet}}$ (Å)	2.237	2.239	2.257
BLD <sub>T</sub>	0.243	0.193	0.128
Volume <sub>T</sub> (Å <sup>3</sup> )	2.32	2.36	2.40
TQE	1.0003	1.0002	1.0003
TAV	1.337	0.747	1.17
$\tau$ (°)	110.415	110.127	110.335
$\alpha$ (°)	8.03	10.18	9.79
$\Delta z$ (Å)	0.023	0.002	0.000
D.M. (Å)	0.536	0.577	0.575
$\Psi_{M1}$ (°)	59.23	58.99	58.00
$\Psi_{M2}$ (°)	59.12	58.91	59.00
BLD <sub>M1</sub>	1.469	0.461	0.589
ELD <sub>M1</sub>	5.390	5.107	5.123
BLD <sub>M2</sub>	3.186	0.722	0.581
ELD <sub>M2</sub>	5.233	5.010	5.115
Shift <sub>M2</sub> (Å)	0.090	0.005	0.008
Volume <sub>M1</sub> (Å <sup>3</sup> )	11.55	11.66	11.78
OQE <sub>M1</sub>	1.013	1.011	1.012
OAV <sub>M1</sub>	41.635	37.521	37.798
Volume <sub>M2</sub> (Å <sup>3</sup> )	11.43	11.59	11.77
OQE <sub>M2</sub>	1.015	1.011	1.012
OAV <sub>M2</sub>	44.435	36.189	38.075
$e_{\text{e},M1}$ (Å)	3.082	3.080	3.090
$e_{\text{e},M1}$ (Å)	2.757	2.770	2.780
$e_{\text{e},M1}/e_{\text{e},M1}$	1.114	1.112	1.108
$e_{\text{e},M2}$ (Å)	3.070	3.071	3.093
$e_{\text{e},M2}$ (Å)	2.753	2.768	2.780
$e_{\text{e},M2}/e_{\text{e},M2}$	1.110	1.109	1.108
toct (Å)	2.115	2.135	2.142
tint (Å)	3.282	3.424	3.457
$\Delta_{\text{K-O4}}$ (Å)	0.367	0.461	0.446
$t_{\text{K-O4}}$ (Å)	3.924	3.942	3.990

Notes:  $t_{\text{tet}}$  = tetrahedral sheet thickness calculated from z coordinates of basal and apical O atoms; TQE = tetrahedral quadratic elongation calculated as  $TQE = \sum (l_i/l_0)^2/4$  where  $l_0$  is the center to vertex distance for an undistorted tetrahedron (Robinson et al. 1971); TAV = tetrahedral angle variance defined as  $TAV = \sum (\theta - 109.47^\circ)^2/5$  (Robinson et al. 1971);  $\tau$  = tetrahedral flattening angle;  $\alpha$  = tetrahedral rotation angle (Hazen and Burnham, 1973);  $\Delta z$  = departure from coplanarity of the basal O atoms, calculated as  $\Delta z = (z_{\text{O2}} - z_{\text{O1}}) \sin \beta$  (Güven, 1971); D.M. = dimensional misfit between tetrahedral and octahedral sheets defined as  $D.M. = [2\sqrt{3} \langle O-O \rangle_{\text{bas}} - 3\sqrt{2} \langle M-O \rangle]$  (Toraya, 1981);  $\psi$  = octahedral flattening angles (Donnay et al., 1964); BLD = bond-length distortions calculated as  $BLD = 100/n * \sum |M-O| - \langle M-O \rangle / \langle M-O \rangle$  (Renner and Lehmann 1986); ELD = edge-length distortion defined as  $ELD = 100/n * \sum |O-O| - \langle O-O \rangle / \langle O-O \rangle$  (Renner and Lehman, 1986); Shift<sub>M2</sub> = off-center shift of the M2 cation defined as the distance between the refined position of cation and the geometrical center of M2 site (coordinates:  $x/a = 0.0$ ,  $y/b = 0.8333$ ,  $z/c = 0.5$ ); OQE = octahedral quadratic elongation calculated as  $OQE = \sum (l_i/l_0)^2/6$  where  $l_0$  is the center to vertex distance for an undistorted octahedron (Robinson et al. 1971); OAV = octahedral angle variance defined as  $OAV = \sum (\theta - 90^\circ)^2/11$  (Robinson et al. 1971);  $e_{\text{e},\text{e}}$  = mean lengths of unshared and shared edges (Toraya, 1981), respectively;  $t_{\text{oct}}$  = octahedral sheet thickness (Toraya, 1981);  $t_{\text{int}}$  calculated from the z coordinates of basal O atoms;  $\Delta_{\text{K-O4}}$  =  $\langle K-O \rangle_{\text{outer}} - \langle K-O \rangle_{\text{inner}}$ ;  $t_{\text{K-O4}}$  = projection of K-O4 distance along c\*.

Cruciani 1993 and Waters and Charnley 2002, for a review). Recalculations should be checked carefully by comparison between independent techniques, such as SCXRD and, when possible, spectroscopic methods. As noted above, these problems arise from the crystal-chemical complexity of micas, because a number of important parameters for formula recalculation (OH concentration, F content, occurrence of other light elements,  $\text{Fe}^{2+}/\text{Fe}^{3+}$  ratio, etc.) may be lacking or poorly-determined.

By combining EMPA and SIMS data, the lower half of Table 1 lists formulae calculated on the basis of 12 (O, OH, F, Cl), and assuming all Fe as  $\text{Fe}^{2+}$  and all Ti as  $\text{Ti}^{4+}$ . Note that octahedral vacancies are negligible for LC7-3Go and LC7-27Go but not for LC7-1R. Indeed, the low octahedral cation sums for spot “a” of LC7-1R and spots “a”, “b”, “c” of sample LC7-27Go, are

related to an unsatisfactory estimate of F and H, which result in a sum of (OH, Cl, F) markedly greater than 2 apfu (see the last row of Table 1). For this reason, crystal-chemical formulae of Table 2 have been calculated only from: spot “c” for LC7-1R, the average over spots “a”, “b”, “c”, “d” for sample LC7-3Go, and spot “d” for sample LC7-27Go.

A crystal-chemical model was applied to sample LC7-1R, which was developed for micas bearing octahedral vacancies (Scordari et al. 2004). This model constrains the distribution of high-charge cations and the  $\text{Fe}^{2+}/\text{Fe}^{3+}$  ratio by estimating the minimum  $\text{Fe}^{3+}$  content from bond-strength considerations. In particular, the model has the following implications: (1)  $M^{3+} \geq 2 \text{Ti}^{4+}$  apfu; and (2) trivalent cations involved in the first implication are distributed over the M2 site, together with Ti and vacancy. Full details of the model and its applications will be reported elsewhere.

For LC7-1R, we found a complex substitution pattern. In particular, 45% of the total Fe must be  $\text{Fe}^{3+}$  to obtain 0.40 atoms per formula unit. The  $\text{Fe}^{3+}$  content and the 0.38  $^{IV}\text{Al}^{3+}$  apfu charge compensate the Ti atoms involved in a Ti-vacancy substitution (0.20  $\text{Ti}^{4+}$  plus 0.20  $\square$  per formula unit). Therefore, the overall substitution mechanism requires concomitant occurrence of Ti-vacancy and  $M^{3+}$ -Tschermak-type substitutions and may be described by the following scheme:  $2^{VI}M^{2+} + 2M^{2+} + 2\text{Si}^{4+} \leftrightarrow ^{VI}\text{Ti}^{4+} + ^{VI}\square + 2^{VI}\text{Fe}^{3+} + 2^{IV}\text{Al}^{3+}$  (Scordari et al. 2004). In addition, a small amount of  $\text{Ti}^{3+}$  (0.02 apfu) is involved with the same amount of  $\text{Li}^+$  in a  $2M^{2+} \leftrightarrow \text{Ti}^{3+} + \text{Li}^+$  substitution; finally 0.03  $\text{Ti}^{3+}$  apfu could be related to 0.04  $\text{O}^{2-}$  apfu in a  $^{VI}M^{2+} + (\text{OH})^- \leftrightarrow \text{Ti}^{3+} + \text{O}^{2-} + 1/2\text{H}_2$ . However, considering that analytical uncertainty for the H and F contents also affects the calculated excess O, it is noteworthy that if the excess O is 0.06 apfu instead of 0.04 apfu, the mechanism is compatible with a  $\text{Ti}^{4+}$ -oxy substitution.

Sample LC7-3Go has the simplest composition. The structural formula is balanced by Ti-Tschermak and  $\text{Al}^{3+}$ -oxy substitution mechanisms. No octahedral vacancies occur in this sample. In LC7-27Go a combination of Ti-Tschermak,  $\text{Al}^{3+}$ -Tschermak, and  $3^{VI}M^{2+} \leftrightarrow 2^{VI}\text{Al}^{3+} + ^{VI}\square$  substitutions occur at the octahedral sites, whereas a minor component of tetraferri-phlogopite likely affects the tetrahedral site.

Crystal-chemical formulae were also calculated using EMPA and SIMS data but with other normalization schemes (see Table 2). The “7 cations method” provided results similar to those obtained with 12 (O, OH, F, Cl) for samples bearing no or negligible octahedral vacancies. The method developed by Dymek (1983) tries to overcome the lack of an  $\text{Fe}^{2+}/\text{Fe}^{3+}$  measurement, but is limited by the assumption of the Ti-vacancy and  $3M^{2+} \leftrightarrow 2\text{Al}^{3+} + \square$  octahedral-substitution occurrence.

Different normalization schemes (Table 2) mainly affects cation populations at octahedral sites and also at tetrahedral sites in some cases, leading to major discrepancies with the structure refinement data. In Table 7, octahedral cation distributions derived from crystal-chemical formulae based on 12 (O, OH, F, Cl) are compared with structure refinement data (mean atomic numbers and bond distances). Calculated bond distances (with the subscript EMPA) were obtained by combining EMPA-derived molar fractions and ionic radii of Shannon (1976). A good agreement between chemical composition and structural features generally exists for all samples.

**TABLE 7.** Octahedral cation distribution, mean atomic numbers (m.a.n., e<sup>-</sup>) of cation sites, octahedral and tetrahedral mean distances, as determined by structure refinement (Xref) and chemical determinations (EMPA)

	Sample			
	LC7-1R	LC7-3Go		LC7-27Go
	Octahedral cation distribution			
	M1:(Mg <sub>0.75</sub> <sup>2+</sup> Fe <sub>0.06</sub> <sup>2+</sup> Fe <sub>0.17</sub> <sup>3+</sup> Li <sub>0.02</sub> )	M1:(Mg <sub>0.76</sub> <sup>2+</sup> Fe <sub>0.16</sub> <sup>2+</sup> Ti <sub>0.08</sub> <sup>4+</sup> )	M1:(Mg <sub>0.82</sub> <sup>2+</sup> Fe <sub>0.12</sub> <sup>2+</sup> Al <sub>0.06</sub> <sup>3+</sup> )	
	M2:(Mg <sub>0.45</sub> <sup>2+</sup> Fe <sub>0.21</sub> <sup>2+</sup> Fe <sub>0.115</sub> <sup>3+</sup> Ti <sub>0.025</sub> <sup>3+</sup> Ti <sub>0.10</sub> <sup>4+</sup> □ <sub>0.10</sub> )	M2:(Mg <sub>0.71</sub> <sup>2+</sup> Fe <sub>0.185</sub> <sup>2+</sup> Ti <sub>0.04</sub> Al <sub>0.065</sub> )	M2:(Mg <sub>0.77</sub> <sup>2+</sup> Fe <sub>0.10</sub> <sup>2+</sup> Ti <sub>0.03</sub> Al <sub>0.09</sub> □ <sub>0.01</sub> )	
		M1 octahedron		
M1 e <sup>-</sup> <sub>Xref</sub>	14.92		15.57	13.29
M1 e <sup>-</sup> <sub>EMPA</sub>	15.04		15.04	13.18
<M1-O> <sub>Xref</sub> (Å)	2.067		2.072	2.078
<M1-O> <sub>EMPA</sub> (Å)	2.072		2.080	2.076
		M2 octahedron		
M2 e <sup>-</sup> <sub>Xref</sub>	16.46		15.12	13.32
M2 e <sup>-</sup> <sub>EMPA</sub>	16.60		15.06	13.67
<M2-O> <sub>Xref</sub> (Å)	2.060		2.067	2.079
<M2-O> <sub>EMPA</sub> (Å)	2.071		2.074	2.066
		Interlayer site		
e <sup>-</sup> <sub>(M1+2M2)Xref</sub>	47.84		45.81	39.93
e <sup>-</sup> <sub>(M1+2M2)EMPA</sub>	48.24		45.16	40.52
		Tetrahedral site		
Ke <sup>-</sup> <sub>Xref</sub>	18.62		19.38	18.92
Ke <sup>-</sup> <sub>EMPA</sub>	18.94		18.48	19.89
Te <sup>-</sup> <sub>Xref</sub>	13.34		14.00	14.00
Te <sup>-</sup> <sub>EMPA</sub>	13.78		13.67	13.87
<T-O> <sub>Xref</sub>	1.654		1.662	1.672
<T-O> <sub>EMPA</sub>	1.667		1.663	1.664

Note: See text for details.

For sample calculations involving the LC7-1R, crystal-chemical formula and cation distribution (see Tables 2 and Table 7) lead to: (1) the best charge balance [ $\Sigma$  positive charges = 22.05 valence units (v.u.),  $\Sigma$  negative charges = 22.03 v.u.]; (2) the best agreement between EMPA-calculated and structure-refinement (Xref)-derived mean atomic numbers, see Table 7; and (3) a good agreement between observed (from Xref) and calculated bond distances (see Table 7). However the crystal chemical model (see above) requires the following cation distribution: M1(Mg<sub>0.75</sub><sup>2+</sup> Fe<sub>0.18</sub><sup>2+</sup> Fe<sub>0.05</sub><sup>3+</sup> Li<sub>0.22</sub><sup>+</sup>); M2 (Mg<sub>0.45</sub><sup>2+</sup> Fe<sub>0.15</sub><sup>2+</sup> Fe<sub>0.175</sub><sup>3+</sup> Ti<sub>0.025</sub><sup>3+</sup> Ti<sub>0.10</sub><sup>4+</sup> □<sub>0.10</sub>). The latter distribution provides the same EMPA-derived mean atomic number per site as that of Table 7 but <M1-O><sub>EMPA</sub> = 2.088; <M2-O><sub>EMPA</sub> = 2.066 Å, so that the agreement between observed and calculated distances improves for the M2 site, but is worse for the M1 site. The unusually high distortion of the M1 site for this sample may play a role in determining this discrepancy (See Table 6, values of bond length distortions for M1, and the section below).

The shorter observed tetrahedral mean bond distance for sample LC7-1R is related to its high F content (see below), whereas the longer <T-O> bond length observed for sample LC7-27Go is consistent with the minor content of tetra-ferriphlogopite component (see Table 2). As further support for LC7-27Go, the <O3-O3> distance is 3.086 Å, quite close to that found by Brigatti et al. (1996, 2003) for tetra-ferriphlogopites (3.091 Å). The <O3-O3> values for LC7-1R and LC7-3Go are 3.065 and 3.068 Å respectively, closer to typical values of phlogopite (Joswig 1972).

Note also that the analysis of geometrical features of M1 and M2 octahedra (Table 5) shows a homo-octahedral nature (Đurović 1981, 1994) of the samples under examination, the differences between <M1-O> and <M2-O> being negligible within the standard deviation. On the other hand, LC7-1R seems to be meso-octahedral when mean atomic numbers are taken into account (Table 7).

Similar features have been observed in a previous work on Mt. Vulture trioctahedral micas (Schingaro et al. 2001).

### Structural features

LC7-1R exhibits cell parameters (in particular *b* and *c*, see Table 3) significantly lower than the other two samples. The shorter *b* parameter is justified by: (1) a lower mean T-O distance; and (2) a lower ditrigonal rotation  $\alpha$  for this sample (see Tables 5 and 6) consistent with values for trioctahedral micas-1M (Donnay et al. 1964). The above features are related to the structural distortion induced by OH  $\leftrightarrow$  F substitution (Boukili et al. 2001). However, the high Ti and F contents are both related to the observed shortening of the *c* cell edge. In particular, trioctahedral micas affected by Ti-oxy substitution exhibit the following structural features: (1) shortening of the *c* edge; (2) shortening of the K-O4 distance; (3) high values of bond length distortions (BLD) for M2, see Table 6; (4) high values of the shift of the M2 cation from the geometric center of the octahedron toward the O4 atom; and (5) low values for  $\Delta_{K-O4}$  (Cruciani and Zanazzi 1994; Cesare et al. 2003; Schingaro et al. 2005). The decrease of the *c*-parameter as the OH  $\leftrightarrow$  F substitution increases was found by Noda and Ushio (1965) and Boukili et al. (2001) in synthetic trioctahedral micas. The explanation of such behavior is straightforward because, as the hydrogen content in trioctahedral micas diminishes by different mechanisms, the K<sup>+</sup>-H<sup>+</sup> repulsion is strongly reduced, leading to the shortening of the interlayer distance (Giese 1979; Munoz 1984). In addition, structural features like those described in points 1, 2, and 5 above were also observed in fluorophlogopite (McCauley et al. 1973).

In summary, LC7-1R seems to display structural features typical of micas affected by Ti-oxy and OH  $\leftrightarrow$  F substitutions, whereas in the previous section the chemical variation was explained by the coupled occurrence of Ti-vacancy and M<sup>3+</sup>-Tschermak substitutions. Thus, some structural details can be

related to the extent of Ti-substitution in the octahedral sheet, but discriminating among the different Ti-substitution mechanisms is not a trivial task. Indeed, as recently determined in a vacancy-bearing trioctahedral mica from tephritic-foiditic pyroclastics from Mt. Vulture (Scordari et al. 2004), a high Ti content associated with a Ti-vacancy substitution mechanism may lead to structural distortions similar to those from a Ti-oxy substitution. The similarities occur owing to the orientation of the OH-vectors relative to the normal to the (001) plane. The results of the present work seem to confirm this trend. Note also that if it is correct that  $\text{OH} \leftrightarrow \text{F}$  substitution and Ti content affect the *c*-parameter, the influence of the latter seems to be dominant. Indeed by inspection of Tables 2 and 3, it can be seen that the *c*-parameter of LC7-3Go is shorter than that of LC7-27Go despite a higher F content. LC7-3Go has also the lowest Ti content among the samples studied.

Brigatti et al. (2003) have modeled the structural distortions relevant to the octahedral sheet for the 1M mica polytype as a function of several parameters, some of which are dependent on local chemical composition, whereas others depend on the overall layer chemistry. In particular, the M2 site is affected by Ti content in micas along the phlogopite-annite join. Figure 1 (modified from Brigatti et al. 2003) shows that the Mt. Vulture samples follow the general trend of an increase of  $y(\text{M}2)$  as the Ti content increases, the effect being remarkable for Ti-phlogopites affected by Ti-oxy substitution [sample labeled Schingaro et al. (2004) and Cruciani and Zanazzi (1994)]. For LC7-1R, the effect appears enhanced and, because of its high F content, it plots close to Ti-rich dehydrogenated samples (Ohta et al. 1982). Schingaro et al. (2005) observed that as Ti increases in the mica structure, the hexagon defined by the O3-O3 octahedral edges undergoes a rigid translation along [100] toward M2, whereas the O4 oxygen atom displaces along [100] away from M1, causing the M1 site to increase and the interlayer separation to decrease. Also, in sample LC7-1R, the octahedral hexagon undergoes a distortion as a function of the Ti content (Fig. 2) but the O4

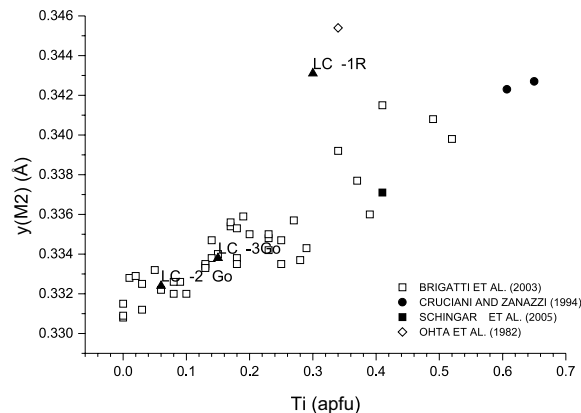


**FIGURE 1.** Variation of  $y(\text{M}2)$  vs. Ti content. Open squares = Ti-phlogopites of igneous origin selected from Brigatti et al. 2003 (their Table 1); filled circles = Ti-rich phlogopites affected by Ti-oxy substitution (samples 21 and 22 from Cruciani and Zanazzi 1994); filled square = Ti-rich ferroanphlogopite affected by Ti-oxy substitution (from Schingaro et al. 2005); open diamond = dehydrogenated Ti-rich biotite (from Ohta et al. 1982); filled triangles = samples under study.

oxygen atom is shifted farther from the interlayer cation and it is displaced toward and not away from M1. This is shown in Figure 3 (modified from Schingaro et al. 2004) where a large negative O4 offset is apparent for sample LC7-1R. Figure 4 plots the displacement of the O4 atom from the center of the hexagon defined by O3 as a function of Ti. Note that Ti-oxy-substituted micas exhibit a positive displacement. In contrast, for sample LC7-1R, the displacement is large and negative and is the greatest displacement in the data set, reflecting the special octahedral compositions of the sample.

By shifting from the center of the O3 hexagon toward M1, the O4 atom causes the M1 site to decrease in size. Indeed, there is no difference in volume between the M1 and M2 sites (see Table 6). In addition, the M1 site is greatly distorted as shown by the analysis of bond length distortion values for M1 in Table 6 and from the sum of the parameters C1 and C2 ( $C1 + C2 = 0.06$  for LC7-1R, 0.003 and 0.014 for LC7-3Go and LC7-27Go, respectively). These latter parameters provide an alternative way to describe the distortion of the M1 site, C1 being dependent mainly on  $y(\text{O}3)$  whereas C2 is affected by  $[x(\text{O}3) - x(\text{O}4)]$  (see Brigatti et al. 2003 for details). As for samples LC7-3Go and LC7-27Go, their geometrical parameters are similar to those

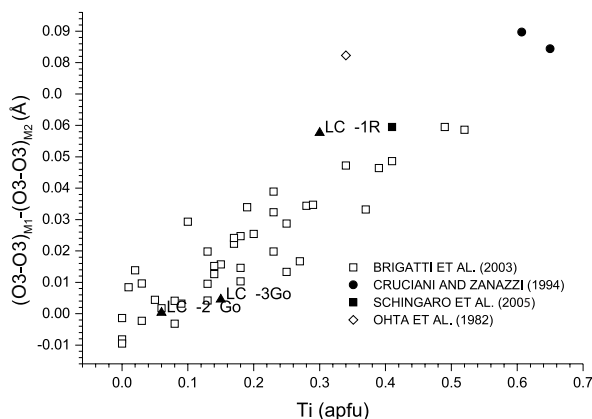


**FIGURE 2.** Effect of Ti over the O3-O3 octahedral hexagon distortion. Symbols as in Figure 1.

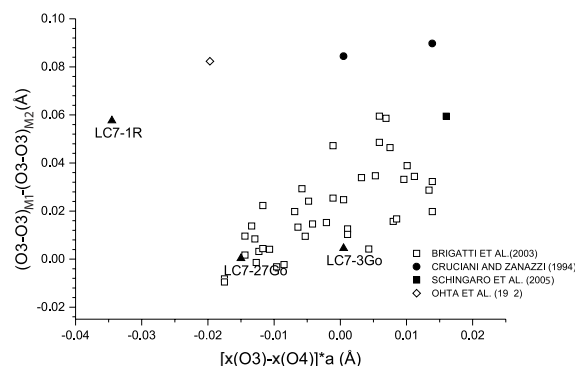


**FIGURE 3.** Relationship between the O3 hexagon distortion and the O4 atom offset from the "octahedral hexagon center". Symbols as in Figure 1.

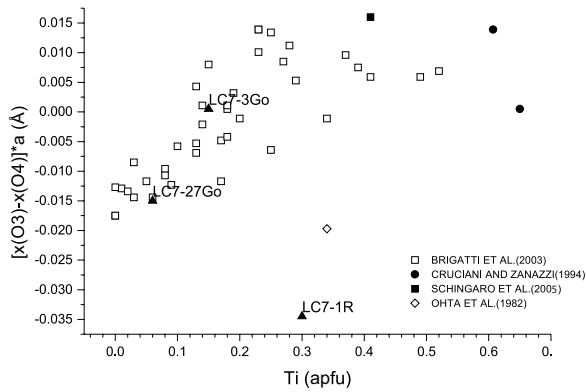


FIGURE 4. Offset of the O4 atom from the “octahedral hexagon center” as a function of Ti. Symbols as in Figure 1.

found in other low-Ti phlogopites (Cruciani and Zanazzi 1994; Brigatti et al. 2003).

#### CONCLUDING REMARKS

Different trioctahedral *1M* mica populations occur at Mt. Vulture. The micas are phlogopite-annite solid solutions with a minor component of brittle micas (kinoshitalite-ferrokinoshitalite solid solutions) and can be distinguished on the basis of their  $X_{Mg}$  values and on their relative contents of Ti and F. All the analyzed samples have  $(OH + F) \sim 2$  apfu so that the oxy-type of substitution plays a very minor role. Titanium uptake in the mica structures occurs via different substitution mechanisms: Ti-Tschermak for Li-, Ti-, and F-poor composition, a combination of Ti-vacancy and Al-Tschermak for Ti-, Li-, and F-rich compositions. However, chemical and structural details show remarkable variations between the red (Ti- and F-rich) and green micas and within the green (Ti- and F-poor) micas. This variability cannot be related to evolution of the Mt. Vulture pholinitic-trachytic volcanics by crystal/liquid fractionation. More complex processes, such as magma mixing and/or interactions with aqueous fluids should be invoked, as suggested by De Fino et al. (1986) and Caggianelli et al. (1990).

Structural effects resulting from Ti in the mica structure also were analyzed. In Mt. Vulture micas, Ti occurs by Ti-vacancy and Ti-Tschermak substitution mechanisms. The results of this work indicate that some structural distortions observed in Ti-vacancy-affected micas are similar to those produced by a Ti-oxy substitution (e.g., shortening of the *c* parameter), whereas others (relative displacements of O3 and O4 atoms positions) are not. However further investigations are needed to determine the response of the mica structure to the different ways of Ti incorporation.

#### ACKNOWLEDGMENTS

Philippa Timmins is gratefully acknowledged for performing data collection of the LC7-1R sample at the Oxford-Diffraction Laboratories. The authors are grateful to Mr. Marcello Serracino for assistance during electron probe microanalyses at the Istituto di Geologia Ambientale e Geoingegneria, CNR, Rome. Detailed reviews by S. Guggenheim, J.M. Hughes, and an anonymous reviewer greatly improved the final manuscript. This work was supported by the COFIN-MIUR (2002). The Consiglio Nazionale delle Ricerche (CNR) is acknowledged for financing the SIMS laboratory at CNR, IGG, Pavia.

#### REFERENCES CITED

- Balenzano, F., De Marco, A., Loiacono, F., and Scordari, F. (1983) Osservazioni preliminari sui caratteri sedimentologici, mineralogici e cristallografici (anfibioli) dei depositi limno-vulcanici del bacino di Atella (M. Vulture). *Adriatica Editrice-Bari*, 26 pp.
- Boukili, B., Robert, J.L., Beny, J.M., and Holtz, F. (2001) Structural effects of  $OH \rightarrow F$  substitution in trioctahedral micas of the system:  $K_2O-FeO-Fe_2O_3-Al_2O_3-SiO_2-H_2O-HF$ . *Schweizerische Mineralogische und Petrographische Mitteilungen*, 81, 55–67.
- Brigatti, M.F. and Guggenheim, S. (2002) Mica crystal chemistry and the influence of pressure, temperature, and solid solution on atomistic models. In A. Mottana, F.P. Sassi, J.B. Thompson, and S. Guggenheim, Eds., *Micas: Crystal Chemistry and Metamorphic Petrology*, 46, 1–100. Reviews in Mineralogy and Geochemistry, Mineralogical Society of America, Chantilly, Virginia.
- Brigatti, M.F., Medici, L., Sacconi, E., and Vaccaro, C. (1996) Crystal chemistry and petrologic significance of  $Fe^{3+}$ -rich phlogopite from the Tapira carbonate complex, Brazil. *American Mineralogist*, 81, 913–927.
- Brigatti, M.F., Guggenheim, S., and Poppi, M. (2003) Crystal chemistry of the *1M* mica polytype: The octahedral sheet. *American Mineralogist*, 88, 667–675.
- Caggianelli, A., De Fino, M., La Volpe, L., and Piccarreta, G. (1990) Mineral chemistry of Monte Vulture volcanics: Petrological implications. *Mineralogy and Petrology*, 41, 215–227.
- Cesare, B., Cruciani, G., and Russo, U. (2003) Hydrogen deficiency in Ti-rich biotite from anatectic metapelites (El Joyazo, SE Spain): Crystal-chemical aspects and implications for high-temperature petrogenesis. *American Mineralogist*, 88, 583–595.
- Crisci, G., La Volpe, L., and Rapisardi, L. (1983) Pleistocene ignimbrites of Monte Vulture (Basilicata, Southern Italy). *Neues Jahrbuch für Geologie und Paläontologie Monatshefte*, H12, 731–736.
- Cruciani, G. (1993) Studio di cristallografia comparativa su flogopiti *1M* naturali, 154 p. Ph.D thesis, University of Perugia, Italy.
- Cruciani, G. and Zanazzi, P.F. (1994) Cation partitioning and substitution mechanism in *1M* phlogopite: A crystal chemical study. *American Mineralogist*, 79, 289–301.
- De Fino, M., La Volpe, L., Peccerillo, A., Piccarreta, G., and Poli, G. (1986) Petrogenesis of Monte Vulture volcano (Italy): inferences from mineral chemistry, major and trace elements data. *Contributions to Mineralogy and Petrology*, 92, 135–145.
- Donnay, G., Donnay, J.D.H., and Takeda, H. (1964) Trioctahedral one-layer micas. II Prediction of the structure from composition and cell dimensions. *Acta Crystallographica*, 17, 1374–1381.
- Đurovič, S. (1981) OD-character, Polytypie und identifikation von Schichtsilikaten. *Fortschritte der Mineralogie*, 59, 191–226
- (1994) Classification of phyllosilicates according to the symmetry of their octahedral sheets. *Ceramics—Silikaty*, 38, 81–84
- Dymek, R.F. (1983) Titanium, aluminium and Interlayer cation substitutions in biotite from high-grade gneisses, West Greenland. *American Mineralogist*, 68, 880–899.
- Foley, S.F. (1989) Experimental constraints on phlogopite chemistry in lamproites: 1. The effect of water activity and oxygen fugacity. *European Journal of Mineralogy*, 1, 411–426.
- Giese, R.F., Jr. (1979) Hydroxyl orientations in 2:1 phyllosilicates. *Clays & Clay Minerals*, 27, 213–223.
- Güven, N. (1971) The crystal structure of *2M1* phengite and *2M1* muscovite. *Zeitschrift für Kristallographie*, 134, 196–212.
- Hawthorne, F.C., Ungaretti, L., and Oberti, R. (1995) Site populations in minerals: terminology and presentation of results. *Canadian Mineralogist*, 33, 907–911.
- Hazen, R.M. and Burnham, C.W. (1973) The crystal structure of one layer phlogopite and annite. *American Mineralogist*, 58, 889–900.
- Henry, D.J. and Guidotti, C.V. (2002) Titanium in biotite from metapelitic rocks: Temperature effects, crystal-chemical controls, and petrologic applications. *American Mineralogist*, 87, 375–382.
- Joswig, W. (1972) Neutronenbeugungsmessungen an einem *1M*-phlogopit. *Neues Jahrbuch für Mineralogie Monatshefte*, 1–11.
- Kogarko, L.N., Uvarova, Y.A., Sokolova, E., Hawthorne, F.C., Ottolini, L., and Grice, J.D. (2005) Oxykinoshitalite, a new mica from Fernando-De-Noronha Island, Brazil: occurrence and crystal structure. *Canadian Mineralogist*, in press.
- La Volpe, L. and Principe, C. (1989) Stratigrafia e storia eruttiva del Monte Vulture: revisione e aggiornamenti. *Bollettino GNV*, 1989–2, 809–902.
- McCawley, J.W., Newham, R.E., and Gibbs, G.V. (1973) Crystal structure analysis of synthetic fluorophlogopite. *American Mineralogist*, 58, 249–254.
- Munoz, J.L. (1984) F-OH and Cl-OH exchange in micas with application to hydrothermal deposits. In S.W. Bailey, Ed., *Micas*, 13, 469–493. Reviews in Mineralogy, Mineralogical Society of America, Chantilly, Virginia.
- Noda, T. and Ushio, M. (1965) Hydrothermal synthesis of fluorine-hydroxyl phlogopite. Part two: Relationship between the fluorine content, lattice constants and the condition of synthesis of fluorine-hydroxyl-phlogopite. *Geochemistry*

- International, 1, 96–104.
- North, A.C.T., Phillips, D.C., and Mathews, F.S. (1968) A semi-empirical method of absorption correction. *Acta Crystallographica*, A24, 351–359.
- Ohta, T., Takeda, H., and Takéuchi, Y. (1982) Mica polytypism: Similarities in the crystal structures of coexisting 1M and 2M<sub>1</sub> oxybiotite. *American Mineralogist*, 67, 298–310.
- Ottolini, L., Bottazzi, P., and Vannucci, R. (1993) Quantification of Lithium, Beryllium and Boron in Silicates by Secondary Ion Mass Spectrometry Using Conventional Energy Filtering. *Analytical Chemistry*, 65, 1960–1968.
- Ottolini, L., Bottazzi, P., Zanetti, A., and Vannucci, R. (1995) Determination of Hydrogen in Silicates by Secondary Ion Mass Spectrometry. *Analyst*, 120, 1309–1313.
- Ottolini, L., Camara, F., and Bigi, S. (2000) An investigation of matrix effects in the analysis of fluorine in humite-group minerals by EMPA, SIMS and SREF. *American Mineralogist*, 85, 89–102.
- Ottolini, L., Camara, F., Hawthorne, F.C., and Stirling, J. (2002) SIMS matrix effects in the analysis of light elements in silicate minerals: Comparison with SREF and EMPA data. *American Mineralogist*, 87, 1477–1485.
- Ottolini, L., Camara, F., and Devouard, B. (2004) New SIMS procedures for the Characterization of a Complex Silicate Matrix, Na<sub>3</sub>(REE,Th,Ca,U)Si<sub>6</sub>O<sub>13</sub>·2.5H<sub>2</sub>O (Sazhinite), and Comparison with EMPA and SREF Results. *Microchimica Acta*, 145, 139–146.
- Patiño Douce, A.E. (1993) Titanium substitution in biotite: an empirical model with applications to thermometry, O<sub>2</sub> and H<sub>2</sub>O barometries, and consequences for biotite stability. *Chemical Geology*, 108, 133–162.
- Renner, B. and Lehmann, G. (1986) Correlation of angular and bond length distortions in TO<sub>4</sub> units in crystals. *Zeitschrift für Kristallographie*, 175, 43–59.
- Richter, K., Dyar, M.D., Delaney, J.S., Vennemann, T.W., Hervig, R.L., and King, P.L. (2002) Correlations of octahedral cations with OH<sup>-</sup>, O<sup>2-</sup>, Cl<sup>-</sup>, and F<sup>-</sup> in biotite from volcanic rocks and xenoliths. *American Mineralogist*, 87, 142–153.
- Rinaldi, A. (2003) Aspetti cristallografici e strutturali di nicchie triottaedriche nel join flogopite-annite, 163 p. Ph.D. Thesis, University of Bari, Italy.
- Robinson, K., Gibbs, G.V., and Ribbe, P.H. (1971) Quadratic elongation, a quantitative measure of distortion in coordination polyhedra. *Science*, 172, 567–570.
- Schingaro, E. (1993) Caratterizzazione cristallografica di granati titaniferi del M. Vulture (Basilicata): stati di ossidazione e distribuzione degli elementi nei siti cristallografici, 191 p. Ph.D. Thesis, University of Bari, Italy.
- Schingaro, E., Scordari, F., and Ventrucci, G. (2001) Trioctahedral micas-1M from Mt. Vulture (Italy): Structural disorder and crystal chemistry. *European Journal of Mineralogy*, 13, 1057–1069.
- Schingaro, E., Scordari, F., Mesto, E., Brigatti, M.F., and Pedrazzi, G. (2005) Cation site partitioning in Ti-rich micas from Black Hill (Australia): a multi-technical approach. *Clays and Clay Minerals*, 53, N.2, 179–189.
- Scordari, F., Schingaro, E., Ventrucci, G., and Pedrazzi, G. (2004) A Crystal chemical model for Ti-rich phlogopite with octahedral vacancies: the case of a crystal from “Cava Ospizio S. Antonio”, Mt. Vulture (Potenza, Italy). 32<sup>nd</sup> International Geological Congress, Florence, Italy 20–28 August 2004, Abstracts, 549.
- Shannon, R.D. (1976) Revised effective ionic radii and systematic studies of interatomic distances in halides and chalcogenides. *Acta Crystallographica*, A32, 751–767.
- Toraya, H. (1981) Distortions of octahedra and octahedral sheets in 1M micas and the relation to their stability. *Zeitschrift für Kristallographie*, 157, 173–190.
- Virgo, D. and Popp, R.K. (2000) Hydrogen deficiency in mantle-derived phlogopites. *American Mineralogist*, 85, 753–759.
- Waters, D.J. and Charnley, N.R. (2002) Local in polymetamorphic gneiss and the titanium substitution in biotite. *American Mineralogist*, 87, 383–396.
- Watkin, D.J. (1992) CRYSTALS, a programmable program. In H.D. Flack, L. Parkanyi, and K. Simon, Eds., *Crystallographic Computing 6—A Window on Modern Crystallography*. Oxford Science Publications, Oxford.

MANUSCRIPT RECEIVED DECEMBER 22, 2004

MANUSCRIPT ACCEPTED JUNE 17, 2005

MANUSCRIPT HANDLED BY STEPHEN GUGGENHEIM